Numerical Simulations of Acoustic-Vortex Interactions in a Central-Dump Ramjet Combustor

K. Kailasanath,* J.H. Gardner,* J.P. Boris,† and E.S. Oran‡
Naval Research Laboratory, Washington, D.C.

A potentially important source of large pressure oscillations in compact ramjets is a combustion instability induced by the interaction of large-scale vortex structures with the acoustic modes of the ramjet. These interactions have been studied using time-dependent, compressible numerical simulations of cold flow in an idealized ramjet consisting of an axisymmetric inlet and combustor. The simulations indicate a strong coupling between the flowfield and the acoustics of both the inlet and the combustor. Vortex rollup is observed near the entrance to the combustor at the first longitudinal acoustic mode of the combustor. A low-frequency mode is also observed in the simulations. This mode is determined by the acoustics of the inlet and causes major changes in the merging pattern of the vortices.

Introduction

THE problems of instability in ramjet combustors have been attributed to complex, nonlinear interactions among acoustic waves, large-scale vortex structures, and chemical energy release. This paper presents the results of numerical simulations performed to isolate and study the interaction between acoustic waves and large-scale vortex structures in an idealized, central-dump ramjet combustor. The objective is to determine the extent to which acoustic waves influence vortex shedding and merging in a confined geometry.

Detailed numerical modeling of the interactions among the various physical and chemical processes which take place within a ramjet combustor is difficult because of the different length and time scales involved. This has led to the development of zonal modeling techniques in which various regions of the ramjet combustor are modeled separately, with the results then coupled to provide an overall description of the flowfield.[1-3] These models are not truly predictive since they are heavily dependent on a prior knowledge of the flowfield. However, by careful adaptation of the parameters used in such models, successful comparisons to experimental data can be achieved.[3] More recently, numerical simulations have been used to study the flowfield in both axisymmetric centerbody[4] and dump combustors.[5-7] In the numerical study of a dump-combustor flowfield,[5] there was fair agreement between the computed quantities, such as mean axial velocity profiles, and experimental data. These computations predicted a steady solution with a large recirculation zone. However, simulations of a centerbody combustor[4] showed an oscillating flowfield with periodic vortex shedding. Neither of these simulations considered the effects of an exit nozzle or acoustic forcing on the flowfield in the combustor. More recent simulations have considered the effects of exit nozzles[6,7] and acoustic forcing.[6] In an earlier work, [6] numerical simulations were used to study the effects of acoustic waves on the flowfield in an axisymmetric dump combustor with a choked flow through the exit nozzle. Those simulations show the periodic shedding of vortices and the presence of the low-frequency oscillations.

A schematic of the idealized central-dump ramjet combustor used in the simulations is shown in Fig.1. The size of the chamber and mean flow characteristics were chosen to model the experiments presented by Schadow et al.[8] A cylindrical jet with a mean velocity of 50 m/s flows into a cylindrical dump with twice the jet diameter. The length of the dump, which acts as an acoustic cavity, is varied to change the first longitudinal mode frequency. An exit nozzle at the end of the chamber is modeled to produce choked flow.

In this paper, the numerical simulation model and tests of the numerical resolution are discussed first. Then two calculations performed on a nonuniform 40×100 grid are discussed in detail. In the first, no acoustic forcing was imposed on the system. In the second, the first longitudinal acoustic mode of the chamber was excited with an external pressure oscillation. Finally, the results from the simulations are compared to experimental observations.

Numerical Model

The numerical model used to perform the simulations solves the time-dependent conservation equations for mass, momentum, and energy in two spatial dimensions. The algorithm used for convective transport is the flux-corrected transport (FCT) algorithm[9] configured in axisymmetric geometry. This is a conservative monotonic algorithm with fourth-order phase accuracy. It is second-order accurate in time and space. That is, the amplitudes are calculated to second-order accuracy but the phase is calculated to fourth-order accuracy. FCT algorithms are constructed as a weighted average of a low- and high-order finite-difference scheme. During a convective transport timestep, FCT first modifies the linear properties of the high-order algorithm by adding low-order diffusion. This prevents dispersive ripples from appearing, and it ensures that all conserved quantities remain suitably monotonic and positive. FCT then subtracts out the added diffusion in regions away from discontinuities. Thus it maintains a high order of accuracy where it is meaningful while enforcing positivity and monotonicity where it is necessary. With various initial and boundary conditions, this algorithm has been used previously to solve a wide variety of problems in subsonic and supersonic flows.

The calculations presented below are inviscid, that is, no explicit term representing physical viscosity has been included in the model. Also, no artificial viscosity is needed to stabilize the algorithm. There is a residual high-order numerical diffusion present which effectively behaves like a viscosity term for

Received May 14, 1986; presented as Paper 86-1609 at the AIAA/SAE/ASME/ASEE 22nd Joint Propulsion Conference, Huntsville, AL, June 16-18, 1986; revision received Jan. 5, 1987.

*Research Physicist, Laboratory for Computational Physics and Fluid Dynamics. Member AIAA.

‡Chief Scientist, Laboratory for Computational Physics and Fluid Dynamics.

†Senior Scientist, Laboratory for Computational Physics and Fluid Dynamics. Member AIAA.

short wavelength modes on the order of the zone size. Unlike most numerical methods, however, FCT damping of the short wavelength modes is nonlinear. Thus, the effects of this residual viscosity diminish very quickly (much faster than k^2) for the long wavelength modes, which results in a high "effective Reynolds number." This paper focuses primarily on the interaction of the acoustic modes with large-scale vortex structures, an essentially inviscid interaction.

For the calculations presented in this paper, the computational cell spacing was set up initially and held fixed in time. Fine zones were used near the entrance to the combustor (the dump plane) in both the radial and axial directions. In both directions, the cell sizes gradually increased away from the step. In the calculations using a 40×100 grid, the cell size in the axial direction decreased from 8.53 cm at the inlet plane to 0.42 cm at the dump plane, and then gradually increased to 0.50 cm at the rear wall of the combustor (the exit plane). The cell sizes in the radial direction increased from 0.15 cm at the step to 0.167 cm at both the axis and the outer wall of the combustor. The effects of numerical resolution were checked by comparing calculations with 20×50, 40×100, and 80×200 cells. These grids were generated by either doubling or halving the cell sizes used in the 40×100 grid.

Boundary Conditions

The proper specifications of boundary conditions are critical for this problem because boundary conditions could be a source of spurious acoustic waves in the flowfield. The initial thrust of the modeling effort was to develop appropriate inflow and outflow boundary conditions.[6,10] In addition to the inflow and outflow, boundary conditions are required at all of the walls and the centerline (or axis) of the combustor. At the solid walls, the normal fluxes are set to zero and the pressure is extrapolated to the normal stagnation condition. No condition is imposed on the tangential velocity at the walls because viscosity is not explicitly included in the calculations. At the axis of the combustor, symmetry conditions are imposed because the calculations are axisymmetric.

At the subsonic inflow, only three conditions can be specified. In addition to specifying the flow direction to be axial, the mass flow rate and the momentum flow rate are specified. This allows the pressure at the mouth of the inlet to fluctuate. Other combinations of boundary conditions were tried, such as holding the pressure constant and specifying the mass flow rate and flow direction. In general, these resulted in the generation of spurious acoustic waves at the boundaries. As a test of the inflow boundary conditions, a planar acoustic source of a prescribed frequency was imposed at the rear boundary and the pressure fluctuations in the inlet were monitored. Using the set of boundary conditions chosen, the pressure at the mouth of the inlet varied with a constant amplitude and frequency which corresponded to that of the acoustic source.[6,10] This test showed that the boundary conditions used allow acoustic waves to reflect without amplification or damping at the inflow. In simulations of different practical combustors, it might be necessary to modify the inflow boundary conditions to allow for partial damping of acoustic waves, or to model the interactions between acoustic waves and the inlet shock.[11,12] Such considerations are beyond the scope of this investigation of the flowfield in an idealized ramjet combustor. Here the emphasis is on modeling the combustor in detail, assuming the inlet configuration to be simple. Further calculations will consider the details of the inlet, such as the presence of the terminal shock.

At the outflow boundary, only one condition can be specified. In general, the pressure within the combustor will be high enough that the outflow through a nozzle at the exit plane will be choked. The computational advantage of this observation is that the outflow can be modeled without actually calculating the details of the flow in a nozzle. In the computations, the flow exits through a number of cells in the exit plane of the combustor at the local sonic velocity. This is implemented by defining the fluid properties in a "guard cell" just outside the exit plane to force the flow to be sonic at the interface between the guard cell and the last computational cell within the combustor.

Results and Discussion

The physical dimensions of the inlet and combustor used in the calculations are given in Fig. 1. The exit consists of an annular ring located at 0.69 D from the axis of the combustor, with an area of 8.69 cm^2. The mass inflow rate is 0.38 kg/s with a mean velocity of 50 m/s. The initial chamber pressure is 186 kPa. These condition were chosen to match those in the experiments of Schadow et al.[8]

The numerical simulations predict values of the density, momentum, and energy for each of the computational cells as a function of time. Using this information, one can selectively generate the data required for various diagnostics such as Fourier analysis, isovorticity contours, and flow visualization. The two diagnostics used most extensively in the analysis presented below are the Fourier analysis of pressure fluctuations at various locations in the dump chamber and instantaneous flow visualization at selected time intervals. Streamlines are primarily used for flow visualization, although density and vorticity contours are also used. The information gained by studying velocity fluctuations has also been used to corroborate and clarify the observations based on the pressure fluctuations.

Based on the mean chamber pressure and density, the frequencies of various acoustic modes possible in the ramjet can be calculated. Some of the lower frequencies (less than 1000 Hz) are associated with the longitudinal modes of the combustor, inlet, or combined system of inlet and combustor. The first longitudinal mode of the combustor alone is 446 Hz while that of the inlet alone is 294 Hz. The first longitudinal mode of the combined system is 177 Hz. Many other complex modes can also result in low frequencies. The transverse and tangential modes are in a higher (greater than 1000 Hz) frequency range. For example, the first radial mode corresponding to the conditions in the calculations presented here is 2587 Hz.

Calculations with and without acoustic forcing were performed. For the calculations with forcing, the first longitudinal acoustic mode was excited at various amplitudes by imposing a time-dependent source of pressure and acoustic energy at the rear wall of the chamber. The source is nearly planar since the entire area inside the annular exit was forced. In all of the calculations presented here, the frequency of the source is 446 Hz, which corresponds to the first longitudinal acoustic mode of the dump chamber.

Test of Numerical Resolution

The grid size required to resolve the important features of the flowfield was determined by comparing calculations with three different grids: 20×50, 40×100, and 80×200. The instantaneous flowfields observed with the three different resolutions are shown in Fig. 2. In this figure, the quantities are plotted as if the cells were evenly spaced; thus, the figure is not to scale. Figure 1 shows the actual physical dimensions of the system modeled, and later in this paper the flowfield is shown to true scale. Displaying the results as in Fig. 2 helps to bring out the similarities and differences between the calculations using the three different grid resolutions.

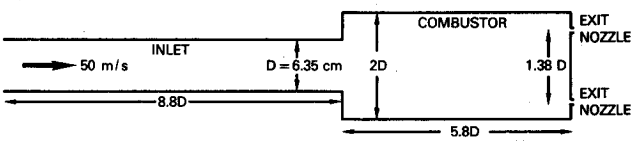

Fig. 1 Configuration of idealized axisymmetric ramjet combustor.

Figure 2 shows that the large-scale structures are essentially the same with the 40×100 and 80×200 resolutions. The 20×50 resolution is too coarse to resolve the finer structures resolved by the other two calculations. The 40×100 grid appears to be adequate to resolve the instantaneous flowfield. Further, the solution on the 20×50 grid eventually settles down to a steady solution with a large recirculation zone, while the solutions with the finer grids show a quasi-steady periodic flowfield with vortex shedding and merging.[10] As a further check on the 40×100 grid, the flowfields at a later stage in the calculations are shown in Fig. 3. Here both the streamlines and contours of constant density are shown. Again, the agreement between the two calculations is good. With the finer 80×200 grid, smaller structures and higher frequencies can be resolved than with the coarser (40×100) grid. The differences in detail are due to fluctuations caused by the smaller-scale structures associated with the finer grid resolution and represent in some statistical sense the limit of accuracy of a finite-difference calculation. However, the dominant frequencies in the periodic flowfield have been shown to be essentially the same with the two resolutions.[10]

Calculations Without Forcing

An unforced calculation on a 40×100 grid is discussed first. The calculations were run for a long time (60,000 timesteps) and flow visualization showed that a periodic solution was attained. The pressure fluctuations at a number of axial and radial locations have been calculated and Fourier-analyzed These include locations at the wall, in the shear layer, and along the axis of the combustor. Figure 4 shows the frequency

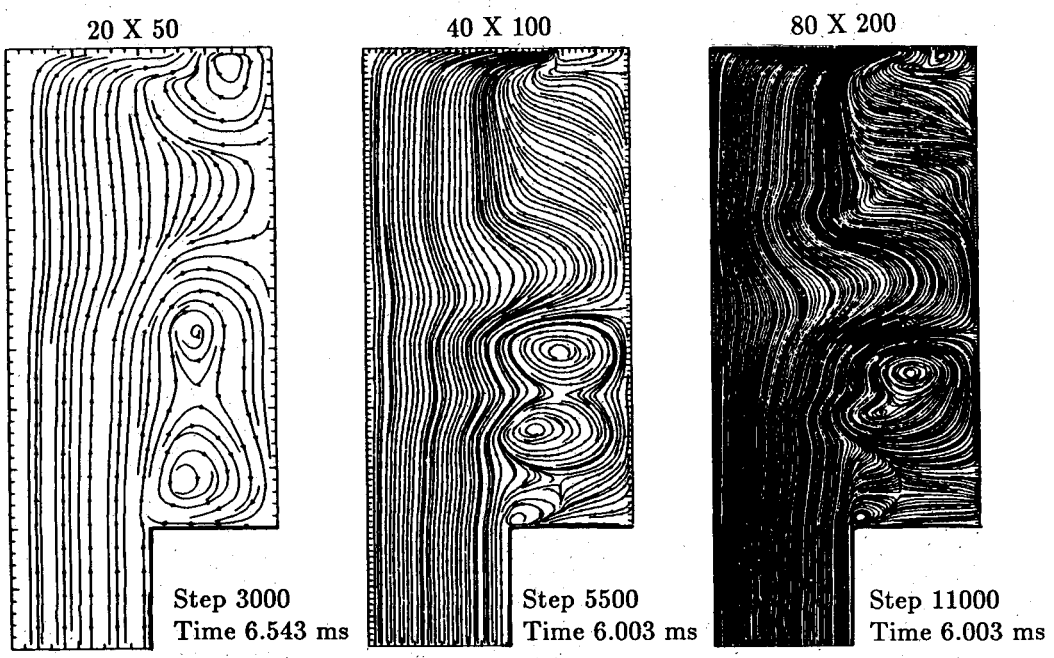

Fig. 2 Comparison of streamlines from calculations with different grid resolutions.

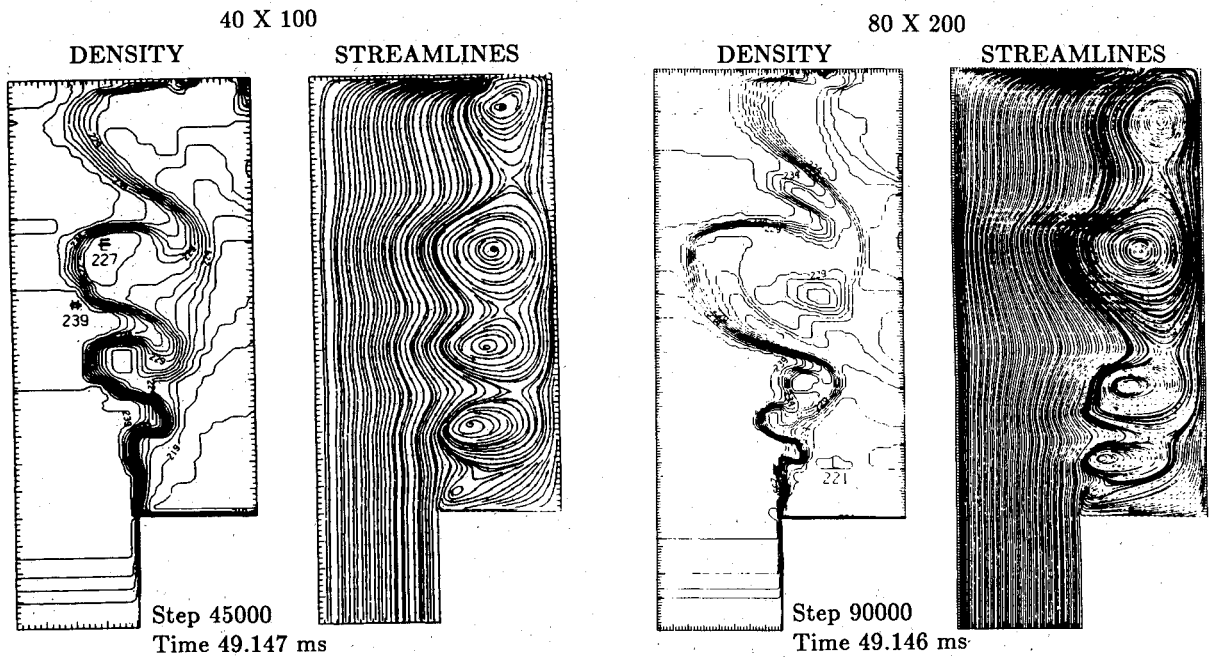

Fig. 3 Comparison of density and streamline contours from calculations using a 40×100 and 80×200 grid.

spectrum at 0.1 and 0.5 D downstream from the dump plane in the shear layer (i.e., at the step height). At both of these locations, the amplitude at about 144 Hz is large. The source of this frequency and its significance is discussed later.

Besides 144 Hz, there is no other dominant frequency at 0.1 D. However, there are also some fluctuations at frequencies between 3000–3500 Hz. These may be associated with transverse acoustic modes of the chamber, though the actual modes corresponding to these frequencies is not clear. At 0.5 D, in addition to 144 Hz, there are also significant amplitudes at about 440 and 880 Hz. The 880 Hz is the initial vortex shedding frequency. Since the 440 Hz peak is highly localized (as evidenced by its not being significant farther upstream or near the walls), it seems to be a characteristic frequency of the shear layer at this position. The 440 Hz is a subharmonic of the vortex shedding frequency of 880 Hz, suggesting that a vortex pairing (or merging) occurs close to the step. However, the details of this pairing process are not clearly resolved in this calculation.

The Fourier analysis of the velocity fluctuations at the same locations, 0.1 D and 0.5 D, is shown in Fig. 5. This figure also shows that the fluctuations at 144 Hz are significant at both locations, but the fluctuations at 440 Hz are significiantly larger at 0.5 D than at 0.1 D. Flow visualization shows the appearance of vortex structures near 0.5 D at a frequency of about 440 Hz. These observations lead to the conclusion that 440 Hz corresponds to pressure and velocity fluctuations associated with vortex structures generated by the most amplified frequency at this position in the shear layer.

Fourier analysis of pressure fluctuations at the corresponding two axial locations at the wall and the centerline of the combustor show much smaller amplitudes near 446 Hz, which corresponds to the frequency of the first longitudinal acoustic mode of the combustor. The appearance of this frequency at these locations indicates that even in unforced calculations there is some modulation of pressure waves by the natural acoustic properties of the chamber.

The effect of the acoustics of the chamber can also be seen by comparing the Fourier analysis of the pressure fluctuations in the shear layer during the early stages (timesteps 5000–15,000) of the evolution of the flow to those at later time. In Fig. 6, the most amplified frequency at 0.5 D is 405 Hz. However, after the flow goes through a number of cycles and the acoustic mode has built up, this frequency shifts to 440 Hz, as seen earlier in Fig. 4. This shift in frequency implies that the acoustics of the chamber play a definite role, even in

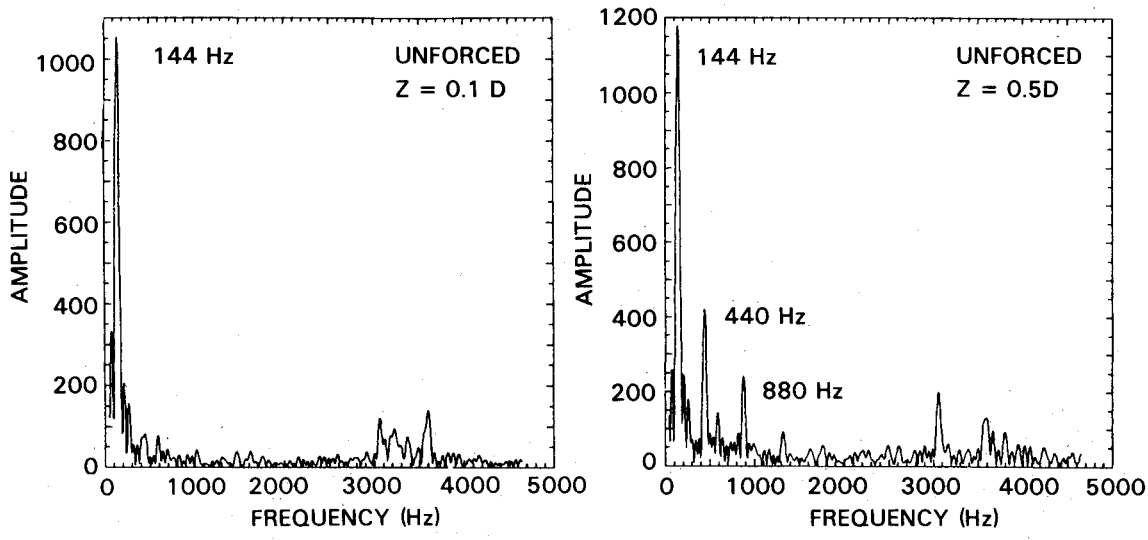

Fig. 4 Frequency spectrum of pressure fluctuations at two locations in the shear layer from the later stages of a calculation without forcing.

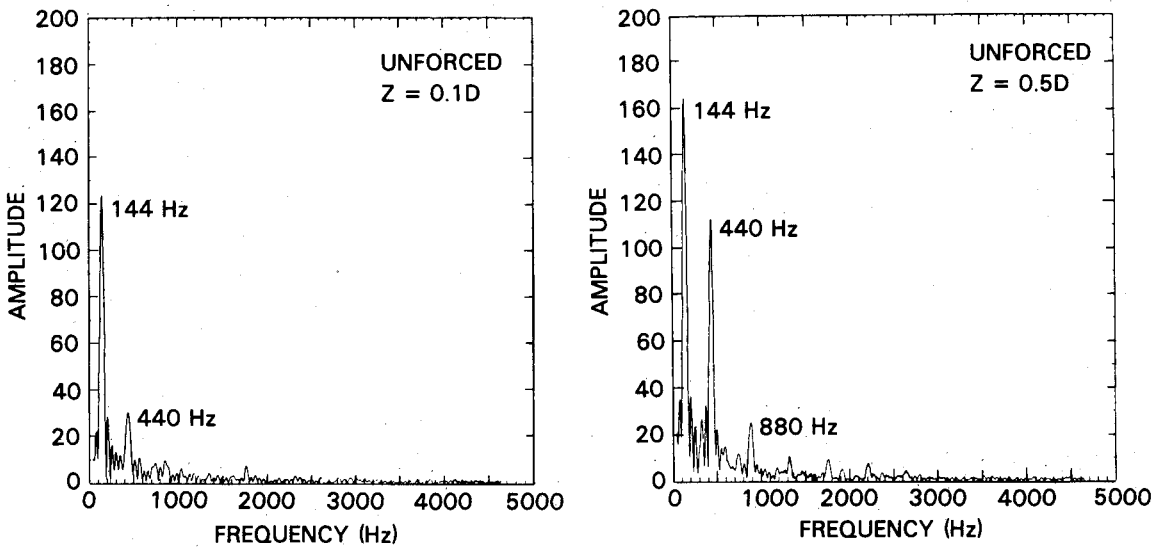

Fig. 5 Frequency spectrum of velocity fluctuations at the same two locations in the shear layer as in Fig. 4.

cases which are not externally forced. In Fig. 6, the amplitudes at frequencies between 3000–3500 Hz are large. Although other calculations have shown that these frequencies are proportional to the diameter of the combustor, the source of these frequencies is not clear. By comparing Figs. 4 and 6, it is seen that these frequencies are significant only in the early stages of the calculations.

Calculations with Acoustic Forcing

Calculations were also performed to study the effects of acoustic forcing on the flowfield. For the case considered here, the amplitude of the imposed acoustic wave was 0.5% of the initial chamber pressure and the frequency of the perturbation was 446 Hz. All other parameters of the calculation were the same as in the unforced case described above. The pressure fluctuations were Fourier-analyzed at the same two axial locations in the shear layer as they were in the unforced case, and the results are shown in Fig. 7. At 0.5 D, the amplitude corresponding to 446 Hz has significantly increased from the unforced value. Higher harmonics of the 446 Hz peak as well as the low-frequency peak at 144 Hz mentioned earlier are also seen. The amplitude corresponding to 446 Hz is even higher at 0.1 D than at 0.5 D. This observation, coupled with the fact that the amplitude at 446 Hz for the unforced case was very weak at 0.1 D, suggests that forcing has not only increased the amplitude of the fluctuations, but has also shifted the location of the shear-layer instability (corresponding to 446 Hz) slightly farther upstream. However, it is also possible that the location has not shifted significantly but the initial rate of growth of the shear layer is significantly higher due to forcing.

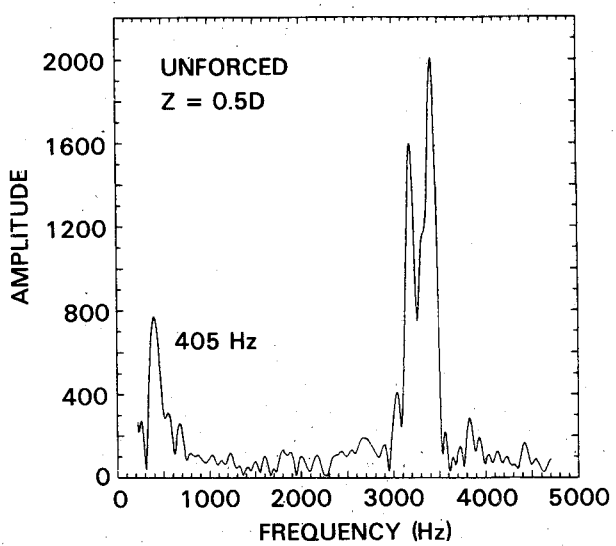

Fig. 6 Frequency spectrum of pressure fluctuations in the shear layer at 0.5 D during the early stages of the calculation without forcing.

The rms velocity fluctuations at 0.1 D for both the forced and unforced cases are shown in Fig. 8 as a function of the radial distance from the centerline of the combustor. The fluctuation level in the region where the vortices are forming (R > 0.5D) is significantly larger in the forced case than in the unforced case. This corroborates the observation made earlier that forcing has resulted in increased fluctuation levels near the step.

Streamline contours of the instantaneous flowfield provide a useful visual diagnostic for studying the structure of the flow. Although the streamline contours show the direction of the flow at a particular instant, the magnitude of the flow velocity is not well represented. Hence, the shape of the vortex structures is well defined while the strengths of the structures are not. As an example, consider Fig. 9, which shows the density and vorticity contours along with the instantaneous streamlines at one particular time (33.86 ms, step 31,000). By this time, the flow has undergone a number of cycles and has settled down to a quasisteady periodic behavior. The vorticity contours show clumps of vorticity centered at about 0.4, 1.3, 2.6, and 5.2 D. These correspond to the vortical flowfield seen in the streamline contours. The density contours show the typical behavior seen in shear flows. Comparing the contours shows the relation between the variations in density, the vorticity contours, and the streamline contours.

Further evidence that forcing at the locally most-amplified frequency produces highly periodic and coherent vortex structures can be seen from studying streamline contours of the instantaneous flowfield. Figure 10 shows the streamline contours within the dump chamber at a sequence of times. The various frames in this figure are instantaneous "snapshots" of the flowfield taken 1.093 ms apart, corresponding to 1000 timesteps in the calculation. The timestep corresponding to each of the frames in the figure is indicated on the left of the frame. In each frame, the dump plane is at the left and the exit plane at the right. The paths of the various vortices are also indicated in the figure. In the first frame (timestep 31,000), a vortex structure is seen near the dump plane. In the second frame (timestep 32,000), this structure has grown and moved downstream. In the third frame (timestep 33,000), not only has this structure moved farther downstream, but a new struc-

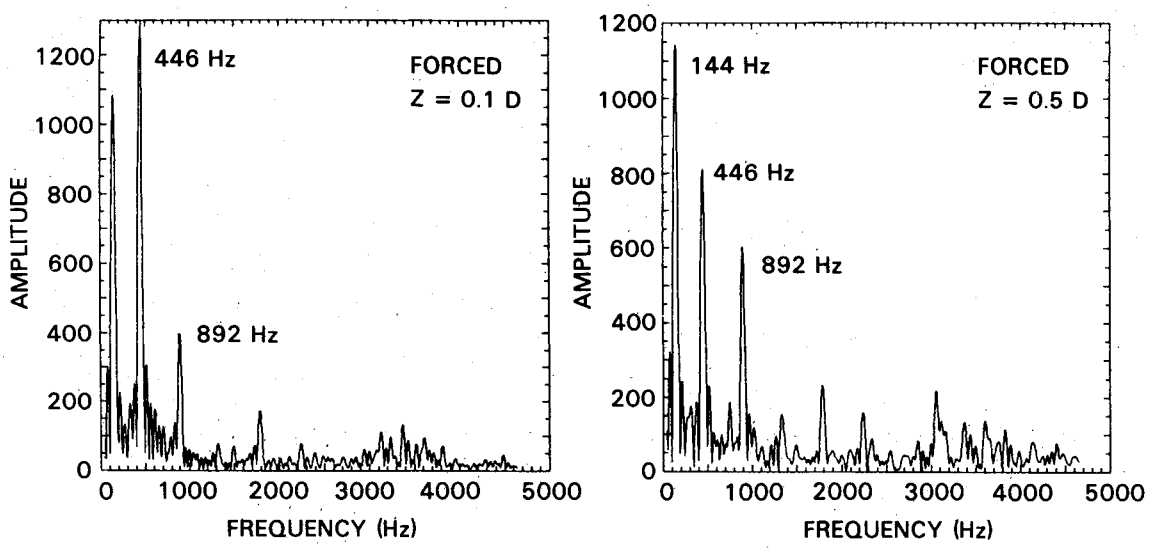

Fig. 7 Frequency spectrum of pressure fluctuations at two locations in the shear layer from the later stage of a calculation with acoustic forcing.

ture has formed near the dump plane. This process continues with a new, large-scale vortex structure appearing near the dump plane at intervals of approximately 2000 timesteps. Thus, in the figure, new large-scale structures appear near the dump plane at timesteps 33,000, 35,000, 37,000, 39,000, 41,000, and 43,000. This corresponds to a frequency of 458 Hz, in close agreement with the Fourier analysis of the pressure fluctuations which gave a frequency of 446 Hz. The small disagreement of 12 Hz is an artifact of showing the flowfield at intervals of 1000 timesteps rather than 1017 timesteps.

Figure 10 shows that the structures which were first seen near the dump plane at timesteps 31,000 and 33,000 have merged (paired) at about 2.4 D by timestep 37,000. As this large, merged structure moves downstream, a new vortex, which was first seen near the dump plane at timestep 35,000, merges with it. This new merging occurs by timestep 43,000 at about 4.8 D. The structures which appeared near the dump plane at timesteps 37,000 and 39,000 merge together at about 2.4 D by timestep 43,000. That is, at either 2.4 D or 4.8 D a merging is observed only at about every 6000 timesteps, which corresponds to a frequency of about 150 Hz. Because new vortices appear near the dump plane every 2000 timesteps, this implies that two successively generated vortices do not always merge with each other.

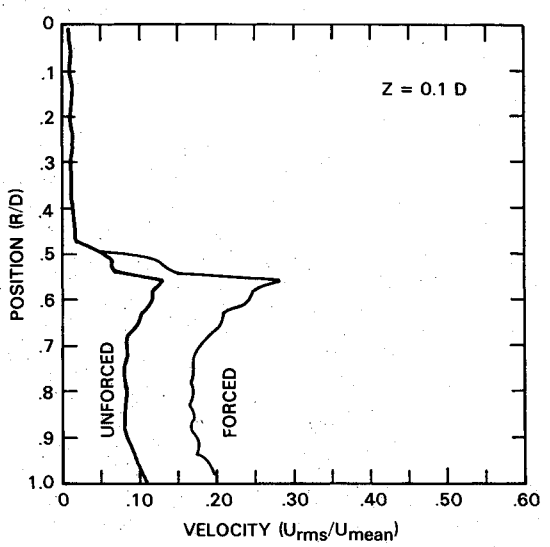

Fig. 8 Comparison of the profiles of the rms velocity fluctuations at 0.1 D from calculations with and without acoustic forcing.

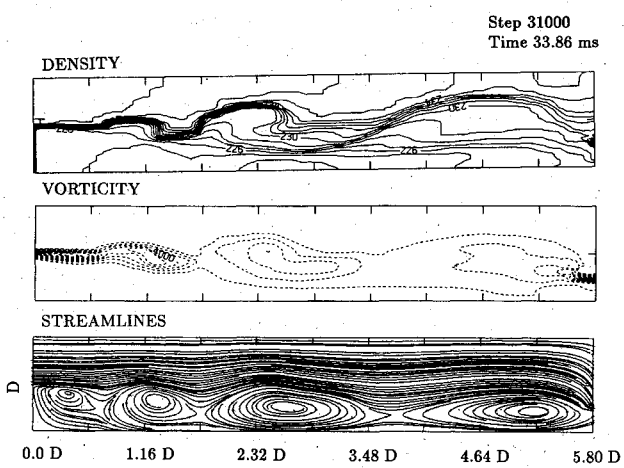

Fig. 9 Density, vorticity, and streamline contours at timestep 31,000 (time = 33.86 ms) from the calculation with acoustic forcing.

The time evolution of the flowfield described above correlates well with the Fourier analysis of the pressure and velocity fluctuations observed at various axial locations in the combustor. The results of Fourier analysis of the pressure fluctuations at the four axial locations, 1.0, 3.0, 4.0, and 5.1 D, are shown in Fig. 11. All of the locations are at the level of the step, a constant radial distance of 0.5 D from the centerline of the combustor. At 1.0 D, 446 Hz is the dominant frequency and this corresponds to the passage frequency of the vortices first seen near the dump plane. This location is similar to 0.5 D since no new major events occur between these two locations. At 3.0 D, a very large amplitude is seen at 144 Hz. The amplitude of this frequency has increased from that at 1.0 D because of the vortex mergings that occur between 1.0 and 3.0 D. In Fig. 10 mergings were observed to occur near 2.4 D at a frequency of 144 Hz. At 3.0 D, a new feature is observed in the spectrum; there is significant amplitude corresponding to 300 Hz. As discussed earlier, two successively generated vortices do not always merge with each other at 2.4 D. Therefore, at 3.0 D, not only does a merged large vortex pass by but also a smaller vortex which will eventually merge

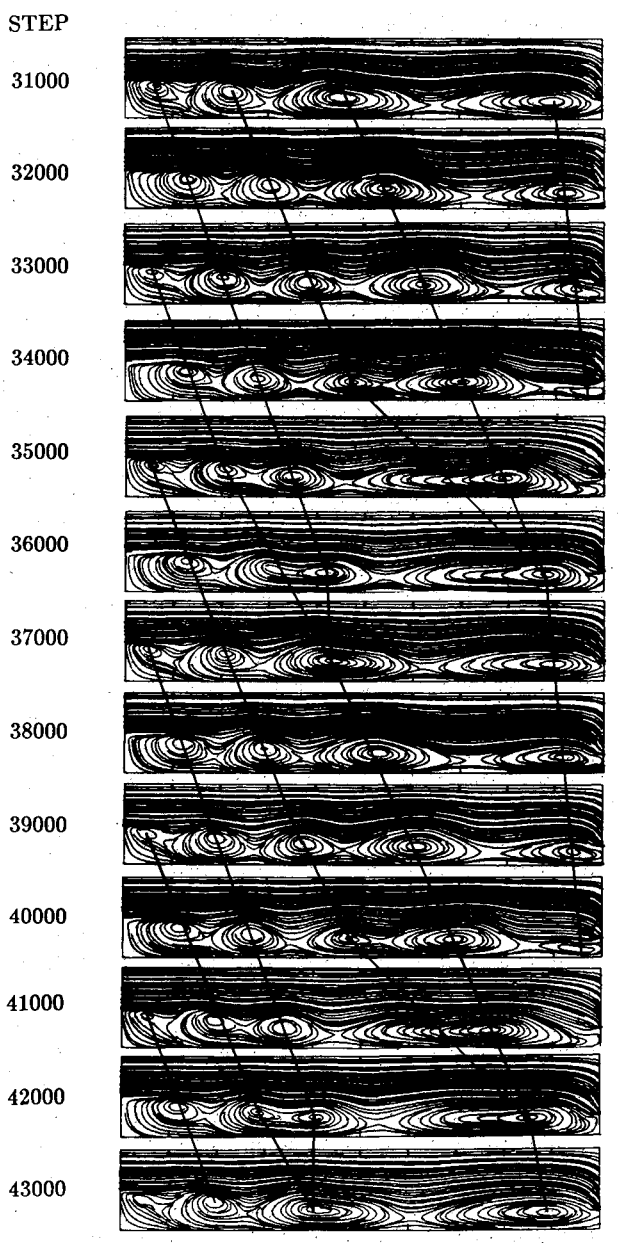

Fig. 10 Streamline contours showing the instantaneous flowfield in the dump combustor at a sequence of timesteps from calculations on a 40 × 100 grid with acoustic forcing.

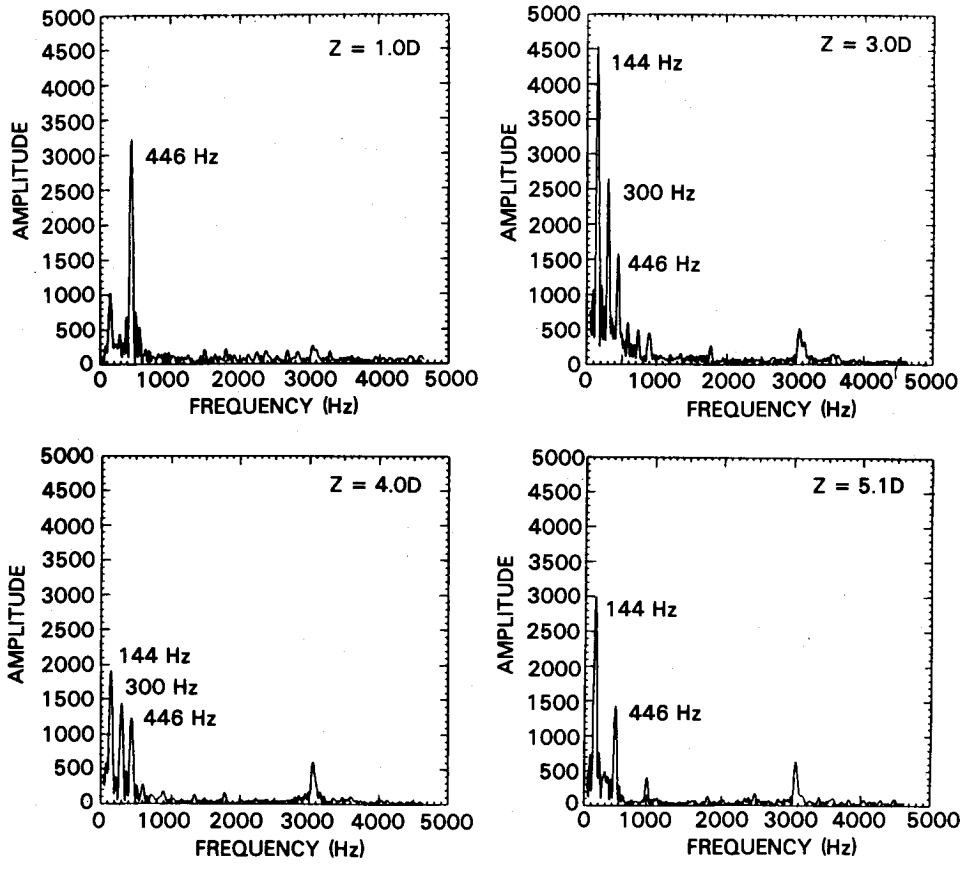

Fig. 11 Frequency spectrum of pressure fluctuations at a series of axial locations in the shear layer from the calculation with acoustic forcing.

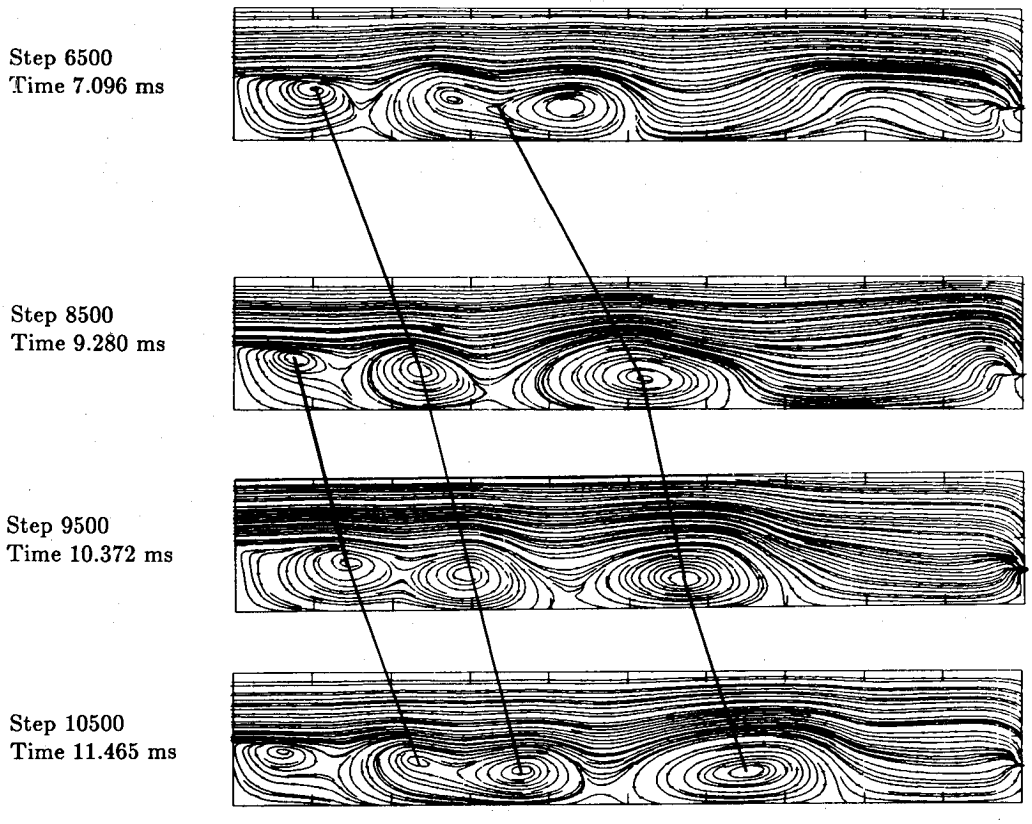

Fig. 12 Instantaneous flowfield in the dump combustor at four timesteps from the early stages of the calculation on a 40 × 100 grid with acoustic forcing.

with the large one near 4.8 D. That is, two vortices pass by 3.0 D during each cycle, resulting in the observed frequency of 300 Hz. Then, as expected, all three frequencies are seen at 4.0 D. At 5.1 D, the amplitude at 144 Hz has increased again because of the mergings which take place near 4.8 D at that frequency. Furthermore, the amplitude at 300 Hz is no longer significant because only one type of large merged vortex will pass by 5.1 D. At all of the locations there is some amplitude corresponding to the forcing frequency of 446 Hz and the low frequency of 144 Hz.

Low-Frequency Oscillations

Figure 10 shows that the entire flow undergoes a complete cycle approximately every 6000 timesteps. For example, at timesteps 33,000 and 39,000 a large-scale structure has partially exited through the nozzle. At these times, the same number of structures of about the same size are seen at about the same locations in the combustor. This similarity exists between any two frames which are 6000 timesteps apart. The frequency corresponding to this cycle is about 150 Hz, which is close to the value of 144 Hz observed in all of the pressure analyses. This also shows that the large-scale flow has settled down to an essentially periodic behavior.

Before this periodic behavior is established, a different kind of merging pattern is observed. In early stages of the calculation, successively generated vortex structures merge with each other. This results in a vortex merging at 2.4 D every 4000 steps, as shown in Fig. 12. The merging frequency estimated from the figure is 229 Hz, which is a subharmonic of the most energetic frequency at the dump plane. This frequency is also close in value to 215 Hz, which was identified by Schadow et al.[8] as the most energetic frequency at about 2.0 D. Once the first vortex begins to exit through the nozzle, this periodicity of the vortex merging is lost and the new periodicity corresponding to about 6000 timesteps (about 144 Hz) is observed.

There are many possible mechanisms that can generate such a low-frequency oscillation. The observation made above that low-frequency oscillations are seen only after the vortices begin to exit the combustor suggests that the interaction between the vortices convecting downstream and the exit nozzle or wall of the combustor may be part of the mechanism that generates the low frequency. Another possibility is that the low frequency is an acoustic mode associated with the inlet. These two mechanisms are examined below.

The interaction between vortices and a surface of impingement as a source of low-frequency oscillations has received considerable attention in the past.[13-15] The basic mechanism has been examined in detail by Ho and Nosseir[13] in their study of the dynamics of a jet impinging on a flat plate. The low-frequency oscillation they observed depended on the convective speed of the vortices, the speed of upstream-propagating waves, and the distance between the jet nozzle and the plate. To examine the similarity between the two phenomena, calculations similar to the simulations discussed above were performed for dump chambers of different lengths. This is equivalent to changing the distance between the jet nozzle and the plate in the Ho and Nosseir[13] experiment. However it was found[16,17] that the frequency of the oscillations was essentially independent of the length of the combustor. Therefore, the interaction between the vortices and the end wall of the combustor does not seem to play a dominant role in determining the low frequency.

As mentioned above, the acoustics of the inlet could also determine the low frequency. The inlet is essentially a long pipe with flow coming in from one end and flowing out into the combustor at the other end. The inflow boundary conditions specified in the numerical model allow complete reflection of the pressure waves that reach the upstream end of the inlet. If the downstream end of the inlet behaves like an open end, the dominant acoustic mode of the inlet would be the quarter-wave mode. Because the length of the inlet is 8.8 D,

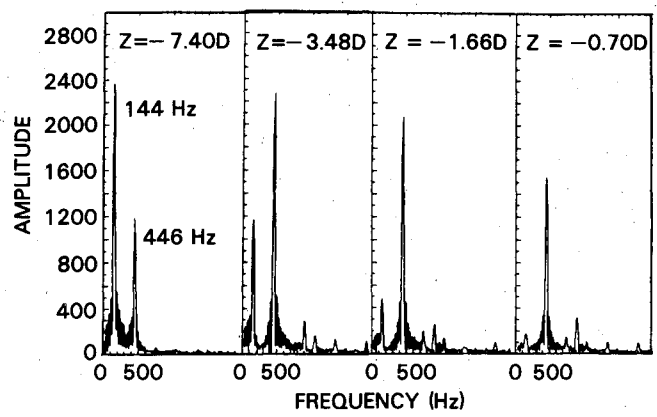

Fig. 13 Frequency specta of pressure fluctuations at four axial locations in the inlet.

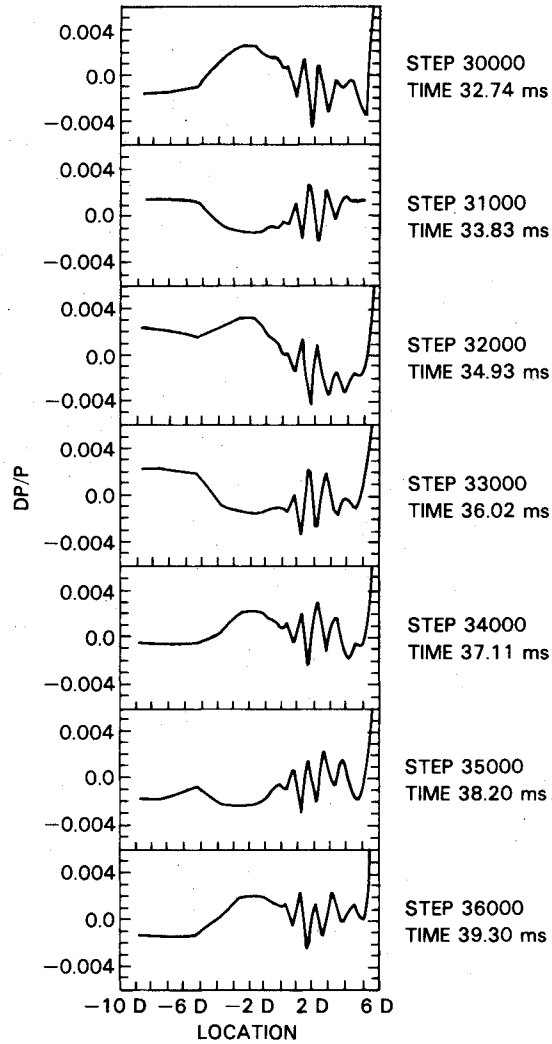

Fig. 14 Axial distributions of pressure fluctuations at a sequence of times.

the frequency of this mode, corresponding to the physical conditions in the simulation discussed above, is about 147 Hz, which is close to the observed frequency of 144 Hz.

In order to study the acoustic modes of the ramjet in greater detail, the Fourier analysis of the pressure fluctuations at various locations in the inlet is shown in Fig. 13. The dominant frequency near the upstream end of the inlet (−7.4 D) is indeed seen to be 144 Hz, but there are also fluctuations at 446 Hz. Closer to the combustor, the amplitude of the 144-Hz mode decreases and that of the 446-Hz mode increases. If the

downstream end of the inlet behaves like an ideal open end, the amplitude at 144 Hz should decrease as one moves toward it and reach zero at the dump plane. This is indeed seen to be the trend.

The spatial distribution of the fluctuating pressure within the inlet and the combustor is shown at a sequence of times in Fig. 14. This shows that the mode in the inlet is not a pure quarter-wave mode. The pressure fluctuation is negative (less than the chamber mean pressure) in the first frame (at 32.742 ms) of the figure. It increases and reaches a postitive maximum between frames 3 and 4 and then decreases to reach a negative minimum between frames 6 and 7. The time interval between frames 1 and 7 is 6.553 ms, giving a frequency of about 153 Hz. That is, the pressure at the upstream end of the inlet goes through a complete cycle at approximately 144 Hz. The pressure distribution near the downstream end of the inlet is essentially the same in every other frame in Fig. 14. This corresponds to a frequency of about 450 Hz.

In order to confirm further that the acoustics of the inlet indeed determines the low frequency, the length of the inlet was decreased to 7.2 D. The low-frequency oscillations appropriately shifted to 180 Hz, which is the frequency of the quarter-wave mode for this inlet. In other simulations,[16] the frequency again shifted appropriately when the sonic speed in the inlet was changed by introducing a heated fuel/air mixture as the inflowing gas.

Conclusions

The results of the calculations presented in this paper indicate a strong coupling between the acoustic modes of the combustor and large-scale vortex structures. In the early stages of the calculations, there is an unforced natural vortex growth near the dump plane at a frequency of 405 Hz. This frequency is close but not equal to the first longitudinal acoustic mode frequency, which is about 446 Hz. As the calculation evolves with time the acoustic modes of the chamber interact with the natural vortex growth so the frequency of the most amplified mode near the dump plane shifts into resonance with the acoustic mode. This is in general agreement with the experimental observations of Schadow et al.[8] in a similar system. They observed that, in their acoustically forced experiments, the most amplified frequency near the dump plane was 460 Hz and the most amplified frequency in a freejet with a similar configuration was 411 Hz. The numerical simulations also indicate that larger velocity fluctuations occur near the combustor step in the forced case than in the unforced case.

An interesting feature seen in these calculations is a low-frequency mode. Pressure oscillations in the inlet indicate that the acoustics of the inlet determines this low frequency. This mode causes major changes in the merging pattern of the vortices, such as the odd pairing of the vortices. Such a low-frequency mode has also been observed in other numerical simulations[6,7] of idealized ramjets. However, this low-frequency mode is not observed in the experimental results reported by Schadow et al.[8] This feature may have been amplified in the calculations by the idealized inlet boundary conditions, which allow for complete reflection of acoustic waves. In more practical ramjet configurations, upstream propagating acoustic waves would interact with the shock in the inlet. The details of this interaction and its effect on the low-frequency mode are currently under investigation.

Acknowledgments

This work was sponsored by the Office of Naval Research and the Naval Air Systems Command. The authors would like to thank Drs. Klaus Schadow, William Clark, and Robert Brown for their many helpful discussions and suggestions. The support and encouragement of Dale Hutchins and Doug Davis are also gratefully acknowledged.

References

[1]Swithenbeck, J., Poll, I., Vincent, M.W., and Wright, D.D., "Combustion Design Fundamentals," *Fourteenth Symposium (International) on Combustion,* The Combustion Institute, Pittsburgh, PA, 1973, pp. 627–636.

[2]Viets, H. and Drewry, J.E., "Quantitative Predictions of Dump Combustor Flowfields," *AIAA Journal,* Vol. 19, April 1981, pp. 484–491.

[3]Edelman, R.B., Harsha, P.T., and Schmotolocha, S., "Modeling Techniques for the Analysis of Ramjet Combustion Processes," *AIAA Journal,* Vol. 19, May 1981, pp. 601–609.

[4]Scott, J.M. and Hankey, W.L., "Numerical Simulation of Cold Flow in an Axisymmetric Centerbody Combustor," *AIAA Journal,* Vol. 23, May 1985, pp. 641–649.

[5]Drummond, J.P., "Numerical Study of a Ramjet Dump Combustor Flowfield," *AIAA Journal*, Vol. 23, April 1985, pp. 604–611.

[6]Kailasanath, K., Gardner, J.H., Boris, J.P., and Oran, E.S., "Acoustic-Vortex Interactions in an Idealized Ramjet Combustor," *Proceedings of the 22nd JANNAF Combustion Meeting*, Pasadena, CA, CPIA Publication 432, Vol. 1, Oct. 1985, pp. 341–350.

[7]Jou, W.H. and Menon, S., "Numerical Simulation of the Vortex-Acoustic Wave Interaction in a Dump Combustor," AIAA Paper 86-0002, Jan. 1986.

[8]Schadow, K.C., Wilson, K.J., Crump, J.E., Foster, J.B., and Gutmark, E., "Interaction Between Acoustics and Subsonic Ducted Flow with Dump," AIAA Paper 84-0530, Jan. 1984.

[9]Boris, J.P. and Book, D.L., "Solution of Continuity Equations by the Method of Flux Corrected Transport," *Methods of Computational Physics*, Academic Press, New York, 1976, Vol. 16, Chap. 11.

[10]Kailasanath, K., Gardner, J.H., Boris, J.P., and Oran, E.S., "Numerical Simulations of the Flow Field in a Central-Dump Ramjet Combustor—I. Tests of the Model and Effects of Forcing," NRL Memo. Rept. 5832, Naval Research Laboratory, Washington, DC, July 1986.

[11]Clark, W.H. and Humphrey, J.W., "Identification of Longitudinal Acoustic Modes Associated with Pressure Oscillations in Ramjets," *Journal of Propulsion and Power*, Vol. 2, May–June 1986, pp. 199–205.

[12]Culick, F.E.C. and Rogers, T., "The Response of Normal Shocks in Diffusers," *AIAA Journal,* Vol. 21, Oct. 1983, pp. 1382–1390.

[13]Ho, C.M. and Nosseir, N.S., "Dynamics of an Impinging Jet. Pt. 1. The Feedback Phenomenon," *Journal of Fluid Mechanics*, Vol. 105, 1981, pp. 119–142.

[14]Flandro, G.A., "Vortex Driving Mechanism in Oscillatory Rocket Flows," *Journal of Propulsion and Power*, Vol. 2, May–June 1986, pp. 206–214.

[15]Abouseif, G.E., Keklak, J.A., and Toong, T.Y., "Ramjet Rumble: The Low-Frequency Instability Mechanism in Coaxial Dump Combustors," *Combustion Science and Technology*, Vol. 36, 1984, pp. 83–108.

[16]Kailasanath, K., Gardner, J.H., Oran, E.S., and Boris, J.P., "Numerical Simulation of Combustion Oscillation in Compact Ramjets," *Proceedings of the 1986 JANNAF Propulsion Meeting*, New Orleans, LA, CPIA Publication 455, Aug. 1986.

[17]Kailasanath, K., Gardner, J.H., Boris, J.P., and Oran E.S., "Acoustic-Vortex Interactions and Low Frequency Oscillations in Axisymmetric Combustors," AIAA Paper 87-0165, Jan. 1987.